

Recurring region for neutron-star observables

ALEXANDER CLEVINGER,¹ ZIDU LIN,^{2,3} MILENA ALBINO,⁴ PETER HAMMOND,^{5,6,7} VERONICA DEXHEIMER,¹ AND
ANDREW STEINER^{2,8}

¹*Center for Nuclear Research, Department of Physics, Kent State University, Kent, OH, USA 44242*

²*Department of Physics and Astronomy, University of Tennessee Knoxville, Knoxville, TN 37996-1200, USA.*

³*Department of Physics and Astronomy, University of New Hampshire, Durham, NH 03824, USA.*

⁴*Department of Physics, CFisUC, University of Coimbra, P-3004 - 516 Coimbra, Portugal*

⁵*Department of Physics, The Pennsylvania State University, University Park, PA 16802, USA*

⁶*Institute for Gravitation and the Cosmos, The Pennsylvania State University, University Park, PA 16802, USA*

⁷*Department of Physics and Astronomy, University of New Hampshire, Durham, NH 03824, USA*

⁸*Physics Division, Oak Ridge National Laboratory, Oak Ridge, TN 37831, USA*

ABSTRACT

In this letter, we report a new phenomena of recurring regions when relating observables for hybrid neutron stars and hybrid neutron-star mergers. To describe dense matter within hybrid stars, we introduce a percolation to vary the size and characteristics of the deconfinement phase transition to quark matter. Before and after the percolation, we keep the hadronic and quark phases the same, described by different realistic models for the equation of state of beta-equilibrated, charge-neutral, zero-temperature matter. When solving spherical and deformed equations for neutron stars in general relativity, we find that: no matter the size or characteristics of the percolation region, or the order of the phase transition on either side (hadronic and quark), as long as we minimize the average sound speed from the beginning of the percolation region to the central density for a given star, we can produce equations of state that cross through the same, small recurring region within mass-radius and mass-tidal deformability diagrams. Our findings provide a new way to produce hybrid equations of state for dense matter that match a given observation of neutron stars or neutron star mergers.

Keywords: neutron star — quark deconfinement — mass-radius diagram — universal relations

1. INTRODUCTION

Within the high densities achieved in the interior of neutron stars, we expect exotic matter to appear within their cores Baym et al. (2018). This comprehends, for example, hadronic matter containing hyperons and Delta baryons and a quark phase containing up, down, and strange quarks (see Appendix A for a quantitative motivation for quark deconfinement). With recent exponential growth of neutron star observations through direct observation of light, as well as gravitational wave observation from their mergers, there is a robust need to build up realistic models for dense matter, while also keeping them consistent with findings from terrestrial laboratory experiments. Exotic matter, particularly strongly interacting deconfined quark matter, is poorly understood and neutron stars can provide us with further insight into the low-temperature, high-density regime of the Quantum Chromodynamics (QCD) phase diagram (see Fig. 1 from Kumar et al. (2023c)). This

means that the deconfinement phase transition could be observed inside neutron stars or during their mergers in the near future, pointing toward the natural (not created in the laboratory) occurrence of deconfined quark matter, as long as we know how to interpret it as such.

In this paper, we work on such interpretation, focusing on hybrid stars that present a second- or third-order phase transition between hadronic and quark matter. We built equations of state (EoSs) using a percolation to describe deconfinement to quark matter Kojo et al. (2015). Such prescription has been motivated by current constraints of nuclear physics and astrophysics that predict structure in the speed of sound of dense matter Tan et al. (2022a); Jakobus et al. (2021); Dexheimer et al. (2015); Alford & Sedrakian (2017); Zacchi et al. (2016); Alvarez-Castillo et al. (2019); Li et al. (2020b); wu Wang et al. (2020); Fadafan et al. (2020); Blaschke et al. (2020); Dutra et al. (2016); McLerran & Reddy (2019); Xia et al. (2021); Yazdizadeh & Bordbar (2019);

Shahrbaf et al. (2020); Zhao & Lattimer (2020); Lopes & Menezes (2021); Duarte et al. (2020); Rho (2021); Marczenko (2020); Minamikawa et al. (2021); Hippert et al. (2021); Pisarski (2021); Sen & Sivertsen (2021); Stone et al. (2021a); Ferreira et al. (2020); Kapusta & Welle (2021); Somasundaram & Margueron (2022); Kojo (2021); Mukherjee et al. (2017); Li et al. (2020a); Jin et al. (2022); Lee et al. (2022); Raduta et al. (2021); Dutra et al. (2012); Dexheimer & Schramm (2010, 2008); Guichon et al. (1996); Malfatti et al. (2020); Bedaque & Steiner (2015); Annala et al. (2020); Stone et al. (2021b); Gusakov et al. (2014); de Paoli & Menezes (2013); Sen (2021); Tu & Zhou (2022); Montaña et al. (2019); Kojo (2019); Malfatti et al. (2019); Jokela et al. (2021); Jeong et al. (2020); Sen & Warrington (2021); Motornenko et al. (2020); Baym et al. (2019); Li et al. (2018); Kumar et al. (2023b); Marczenko et al. (2022); Tews et al. (2018); Fujimoto et al. (2022); Zuo et al. (2022); Braun & Schallmo (2022); Ivanytskyi & Blaschke (2022); Fraga et al. (2022); Huang et al. (2022); Han et al. (2023); Pinto (2023); Kumar et al. (2023a); Liu et al. (2023); Yamamoto et al. (2023); Kouno & Kashiwa (2024); Gao et al. (2024); Tajima et al. (2024); Legred et al. (2022); Altiparmak et al. (2022); Mroczek et al. (2023); Kawaguchi & Suenaga (2024); Cuceu & Robles (2025); Xia et al. (2024); Ye et al. (2025); Kovács et al. (2022). It consists of introducing a polynomial between the hadronic and quark EoSs, increasing the order of the phase transition to a higher one, while modifying the stiffness of the EoS. As a result of our thorough analysis including different EoSs, different orders of phase transitions, and large parameter space sweep, we identified a recurring region, where several different hybrid EoSs cross in the mass-radius diagram and in the mass-tidal deformability diagrams. In the following, we present the feature of recurring regions, identify how to produce EoSs that cross a region determined by a chosen stellar mass and radius or tidal deformability, and discuss how this universal behavior can be used to interpret future observations of neutron stars and neutron-star mergers. We begin by discussing fixed stellar masses, and then discuss how to change the respective radii. The Python scripts used in our work will be made available upon publication.

2. METHODOLOGY

To describe β -equilibrated, charge-neutral, dense zero-temperature hadronic matter, we make use of two realistic microscopic EoS models. First, we consider the Chiral Mean Field (CMF) model, an effective relativistic model which was constructed and fitted to reproduce many features of QCD, including standard neu-

tron star observables Dexheimer & Schramm (2008). We focus on one parametrization from Ref. Clevinger et al. (2022) available on the CompOSE repository Oertel et al. (2017); Typel et al. (2015); Oertel et al. (2017); Typel et al. (2022, 2015), referred to as CMF-7. It includes nucleons, hyperons, Deltas baryons, electrons and muons, combined with additional vector-isovector interactions and is connected to a crust EoS for low densities to describe nuclei Gulminelli & Raduta (2015). The second hadronic EoS is DD2F, a relativistic mean field (RMF) approach with density-dependent couplings and corrections due to flow constraint Alvarez-Castillo et al. (2016). It includes nucleons and a statistical model for the crust Hempel & Schaffner-Bielich (2010).

To describe β -equilibrated, charge-neutral, dense zero-temperature quark matter at zero temperature, we make use of microscopic prescriptions that are already connected to the hadronic EoSs we selected. Ref. Clevinger et al. (2022) already provides a hybrid version of CMF-7 connected to a quark phase containing up, down, and strange quarks (in addition to leptons) through a first-order phase transition Dexheimer & Schramm (2010); Dexheimer et al. (2021). On the other hand, Bastian (2021) connects the DD2F hadronic phase with a phase of up and down quarks described by the The Nambu-Jona-Lasinio (NJL) model used with a string flip model (SFM) term and vector interactions Kaltenborn et al. (2017). Notice that both, the CMF and NJL models, additionally describe the restoration of chiral symmetry, predicted by QCD to take place at high energies Nambu & Jona-Lasinio (1961).

To describe the *process* of deconfinement, we insert a percolation around the first-order phase transition in the different combined hadronic and quark EoSs. We follow the method described in Kojo et al. (2015), which removes the discontinuities associated with the first-order phase transition. The percolation introduces instead two new phase transitions (now of higher order) at the boundaries of a polynomial, whose coefficients are fitted to various boundary conditions. In this work, use fifth order polynomials to describe quark deconfinement.

The idea of percolation was motivated by the quarkyonic picture, based on the idea that between the hadronic and quark phases there is a phase where the baryon structure begins to break down, but the quarks themselves are still somewhat bound to each other McLerran (2020). In the limit that hadrons are made up of quarks with a large number of colors, this is a prediction of QCD. In our Universe, where hadrons are made up of quarks with three colors, quarkyonic matter might still persist and, at low temperatures, such phase could span a large range of densities, corresponding to a

large portion of neutron star interiors. While this percolation method does not allow for a coherent picture of the particle composition within the percolation region, thermodynamically, it provides a middle ground that resembles a quarkyonic phase [McLerran & Pisarski \(2007\)](#).

Our procedure to build the percolation is as follows: 1) we start by choosing for each EoS two values of baryon (number) density n_B to control the beginning and end of the percolation region, $n_{B,H}$ and $n_{B,Q}$, 2) we find the corresponding baryon chemical potentials $\mu_{B,H}$ and $\mu_{B,Q}$ in the hadronic and quark EoSs, and 3) we calculate the pressure in the percolation region using the polynomial,

$$\mathcal{P} = \sum_{m=0}^5 b_m (\mu_B)^m, \quad (1)$$

with 6 coefficients determined by 6 boundary conditions. These conditions are the ones that determine the new order of phase transitions at the boundaries. They are

$$\left. \frac{d^N P_H}{d\mu_B^N} \right|_{\mu_{B,H}} = \left. \frac{d^N \mathcal{P}}{d\mu_B^N} \right|_{\mu_{B,H}}, \quad \left. \frac{d^N P_Q}{d\mu_B^N} \right|_{\mu_{B,Q}} = \left. \frac{d^N \mathcal{P}}{d\mu_B^N} \right|_{\mu_{B,Q}}, \quad (2)$$

where for $N = 0$ these mean that the percolation region pressure matches the EoS pressure on either side (applies even to a first-order phase transition), for $N = 1$ these mean that the first derivatives match (second-order phase transition and higher), and for $N = 2$ these mean that the second derivatives match (third-order phase transition and higher). We note that the n^{th} derivative of the pressure can also be written as the n^{th} -order susceptibility, $\chi_n^B = \frac{\partial^n P}{\partial \mu_B^n} = \frac{\partial^{n-1} n_B}{\partial \mu_B^{n-1}}$. Alternatively, one can also impose specific constraints (beyond Eq. 2) at the boundaries, such as specifying any of the susceptibilities χ_n^B . This allows us to change the size of the discontinuities at the boundaries of the percolation region. In this work, we do exactly that by:

- matching 0th- and 1st-order derivatives at the boundaries and varying χ_2^B on both sides of the percolation region. By doing that, we have a fifth-order polynomial to describe a **second-order phase transition**. The first 4 constraints are fixed by Eq. 2) (with $N = 0$ and $N = 1$)
- matching 0th-, 1st-, and 2nd-order derivatives at the boundaries. By doing that, we have a fifth-order polynomial to describe a **third-order phase transition**. The 6 constraints are fixed by Eq. 2) (with $N = 0$, $N = 1$, and $N = 2$)

Finally, we must also consider whether our newly constructed EoSs are physical. There are several thermody-

namic and astrophysical constraints to consider, in addition to causality (speed of sound less than the speed of light, $= 1$ in natural units). Other constraints at either low or high density are already fulfilled by the original microscopic EoSs. We impose a limit within the percolation region on the speed of sound ($0 < c^2 < 1$), that the pressure must be continuous, and that n_B must be a convex function of μ_B , $\chi_2^B \geq 0$ (see Ref. [Aloy et al. \(2019\)](#) for a discussion of concave EoSs in the context of gravitational waves). The main astrophysical constraint we impose is that the EoS must be able to produce a neutron star with mass $> 2.0 M_\odot$ to be consistent with astrophysical observations of heavy neutron stars [Fonseca et al. \(2021\)](#). This can be checked by solving the Tolman-Oppenheimer-Volkoff (TOV) equations with our constructed EoSs [Tolman \(1939\)](#); [Oppenheimer & Volkoff \(1939\)](#). Other relevant astrophysical observables, such as radius or tidal deformability (which requires solving Einstein field equations with perturbations due to the gravitational field [Hinderer \(2008\)](#)), can also put constraints on producing physical EoSs. However, since the uncertainties on those measurements are much larger, instead of enforcing a specific limit for them as we did for the mass, we only use them as a guide for the discussion of hybrid stars built from EoSs with percolation, more specifically reproducing stellar radii that are not too large. For further discussion on these constraints, see [Kumar et al. \(2023c\)](#).

3. RESULTS

Fig. 1 shows results for several EoSs generated from CMF-7 using our percolation prescription and enforcing the constraints listed above together with small neutron star radii, below ~ 13.5 km [Miller et al. \(2019\)](#); [Riley et al. \(2019\)](#). They are built using different densities on the hadronic and quark percolation boundaries, reproducing different orders for the phase transitions at these boundaries, and imposing different susceptibilities at the boundaries for the case of second-order phase transitions. As seen in the left panel, they all produce bumps in the speed of sound squared (see discussions in the introduction). For the original microscopic CMF-7 EoS, the speed of sound goes to zero, marking the first-order phase transition for deconfinement. The middle panel shows the mass-radius diagram and the right panel shows the mass-tidal deformability diagram for these curves. In both diagrams, we find a recurring region, where several different EoSs with percolation (but not all) cross at a stellar mass near $1.5 M_\odot$.

To investigate this recurring region, we define a new quantity, the average speed of sound squared,

$$c_{\text{avg}}^2 = \frac{P_c - P_H}{\varepsilon_c - \varepsilon_H}. \quad (3)$$

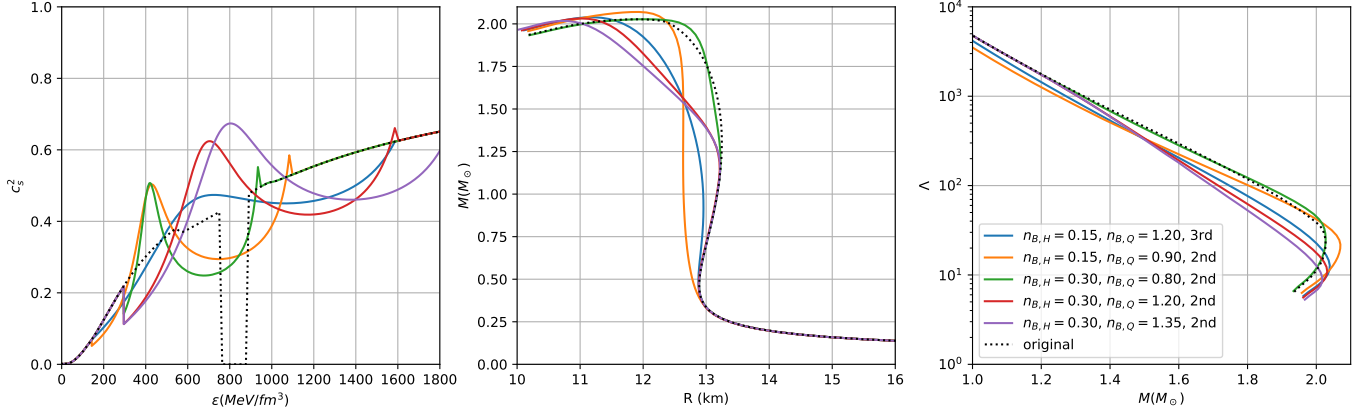


Figure 1. Speed of sound squared for five CMF-7 EoSs with percolation, together with the original microscopic EoS (left panel), corresponding mass-radius diagram (middle panel), and mass-tidal deformability diagram (right panel). The EoSs with percolation are built using different densities on the hadronic and quark percolation boundaries (values shown in fm^{-3}) and reproducing different orders for the phase transitions at these boundaries.

This quantity measures the average speed of sound within the percolation region up to the center of the chosen star. Note that the average speed of sound squared in the entire star has been recently connected to macroscopic stellar properties, such as compactness, through universal relations [Saes et al. \(2024\)](#). As an example, we calculate the average speed of sound from the beginning of the percolation region up to the center of the star for the first EoS with percolation from Fig. 1 (blue curve), corresponding to a third-order phase transition with boundaries $n_{B,H} = 0.15 \text{ fm}^{-3}$ and $n_{B,Q} = 1.20 \text{ fm}^{-3}$, using a stellar mass of $1.554 M_\odot$ (where the recurring region appears in Fig. 1). Then, we modify this EoS by varying widely two constraints, the susceptibilities $\chi_2^{B,H}$ and $\chi_2^{B,Q}$ (turning them into second-order phase transitions), and compare the c_{avg}^2 from Eq. 3 across a large parameter space. The results for the causal and convex EoSs are shown in the top panels of Fig. 2, where the minima in c_{avg}^2 are marked by red dots.

More specifically, the top left panel of Fig. 2 shows the susceptibility at the quark boundary for the percolation in the x-axis and different values for the susceptibility at the hadronic boundary using different line colors. The top right panel shows instead the susceptibility at the hadronic boundary for the percolation in the x-axis and different values for the susceptibility at the quark boundary using different line colors. The lower panels of Fig. 2 show the corresponding stellar radii for the same curves. In the bottom left panel, the radii corresponding to the minima marked by the red dots vary between a small range of $\sim 0.8 \text{ km}$ and in the right panel between a much smaller range of $\sim 0.2 \text{ km}$. Nevertheless, the stellar radii range in the right panel corresponds to values that are too large, outside the current accepted values for astrophysics (see Tab. 10 of [Kumar et al. \(2023c\)](#)), and, there-

fore, were not selected for Fig. 1. The stellar radii range in the bottom left panel of Fig. 2 corresponds to values that are smaller, compatible with astrophysics data, and include the values for the first (blue) curve of Fig. 1 ($\chi_2^{B,H} = 0.00226$ and $\chi_2^{B,Q} = 0.00106 \text{ fm}^{-3}/\text{MeV}$), as expected. Furthermore, the y-axis range corresponding to the red dots in the bottom left panel of Fig. 2 provides a size for the recurring region in Fig. 1 (for a given set of density boundaries for the percolation).

We now repeat the exact same prescription but change the density boundaries for the percolation regions to match the red curve of Fig. 1 for CMF-7 ($n_{B,H} = 0.30 \text{ fm}^{-3}$ and $n_{B,Q} = 1.20 \text{ fm}^{-3}$), still for a star with mass $1.554 M_\odot$. We once more vary the susceptibility at the quark boundary for the percolation in the x-axis and different values for the susceptibility at the hadronic boundary using different line colors (the method used in the left panels of Fig. 2), but now obtain no causal EoSs. We then vary the susceptibility at the hadronic boundary for the percolation in the x-axis and different values for the susceptibility at the quark boundary using different line colors (the method used in the right panels of Fig. 2), and show the results in Fig. 3. The results are qualitatively the same as for the right panels of Fig. 2, but spanning a significantly smaller range of radii of 0.1 km , still in agreement with the recurring region in the left panels of Fig. 2.

For completion, we repeat our calculations for the CMF-7 EoS producing a recurring region for a larger mass of $1.8 M_\odot$. We report the details in Appendix B1 and only summarize them here. We find again 2 recurring regions, as in Fig. 2, but exclude the large radius one due to astrophysical constraints. Still both recurring regions appear at larger radius than for the lower star mass. We also repeat our calculations for different

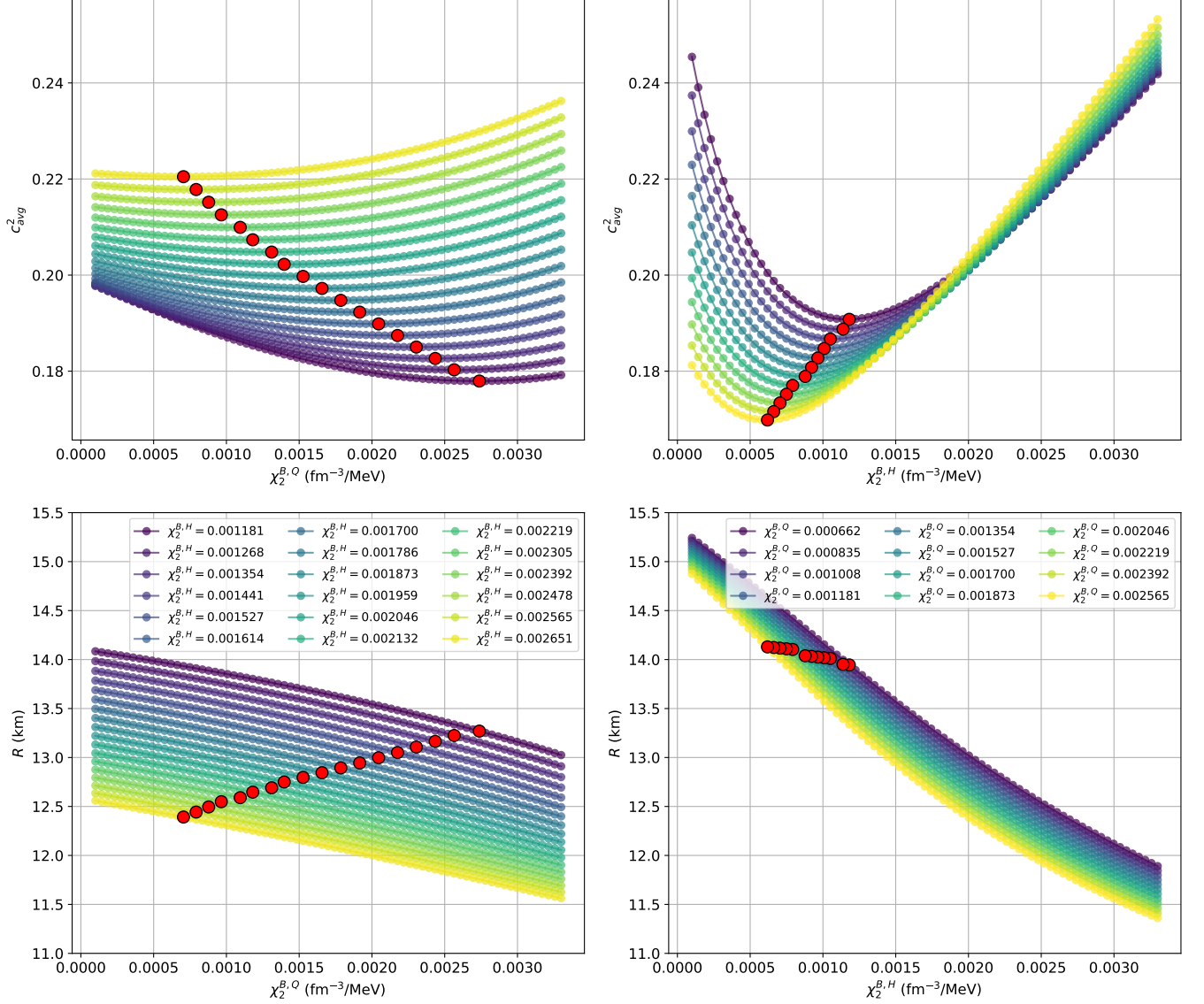


Figure 2. In the top panels, we use the same density boundaries for the percolation regions as the blue curve of Fig. 1 from CMF-7 ($n_{B,H} = 0.15 \text{ fm}^{-3}$ and $n_{B,Q} = 1.20 \text{ fm}^{-3}$) for a star with mass $1.554 M_{\odot}$, but now we show the average speed of sound squared for several different second-order susceptibilities at the boundaries. The top left panel shows the susceptibility at the quark boundary for the percolation in the x-axis and the different susceptibilities at the hadronic boundary using different line colors (values in $\text{fm}^{-3}/\text{MeV}$). The top right panel shows the susceptibilities exchanged. Red dots mark the minimum c_{avg}^2 for each curve. The lower panels show the corresponding stellar radii for the same curves.

hadronic and quark microscopic EoSs, the DD2F-NJL model combination. We report the details in Appendix B2. We choose a star with mass of $1.554 M_{\odot}$ and find again 2 recurring regions, as in Fig. 2, but exclude the large radius one due to astrophysical constraints.

Now that we understand the recurring regions and how to identify them, we can return to discussing Fig. 1. The blue, orange, red, and purple curves have susceptibilities that are close to minima in c_s^2 for a $1.554 M_{\odot}$ star. As a result, these curves pass close enough together to describe a recurring region approximately. This is the

case even though they have different values of $n_{B,H}$ and $n_{B,Q}$ and different orders of phase transition. The red and purple curves have higher $n_{B,H}$ values than the blue and orange curves. This modifies their behavior for low densities (left panel of Fig. 1) and low-mass stars (middle and right panels of Fig. 1). However, again, since their susceptibilities are close to the minima in c_s^2 , the curves pass close to the recurring region. The green curve, however, has susceptibilities that are NOT close to the minima in c_s^2 and, therefore, does not pass close to the recurrent region.

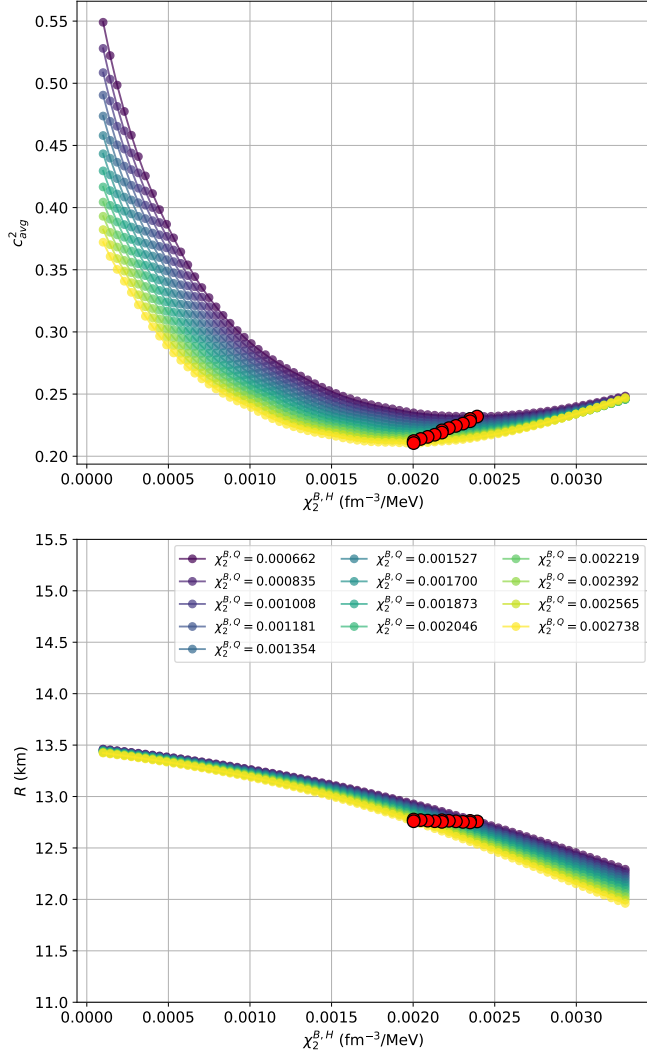


Figure 3. Same as the right panels of Fig. 2, but now for the same density boundaries for the percolation regions as the fourth (red) curve of Fig. 1 from CMF-7 ($n_{B_H} = 0.30 \text{ fm}^{-3}$ and $n_{B_Q} = 1.20 \text{ fm}^{-3}$), still for a star with mass $1.554 M_\odot$.

4. CONCLUSIONS AND OUTLOOK

In this work, we provide a new method to produce realistic dense matter equations of state (EoSs) that cross through a small recurring region in the mass-radius and mass-tidal deformability diagrams. We model quark deconfinement inserting a percolation region between hadronic and quark phases, while changing the order of the phase transition from first to second or third. By minimizing the speed of sound squared from the beginning of the percolation to the center of a given stellar mass, we can select parameters (second order baryon susceptibilities in the hadronic and quark boundaries of the percolation region) that reproduce observables in a recurring region including that given star mass. This

is independent of the densities at which the percolation is inserted and the order of the phase transition at the percolation boundaries. Changing the hadronic side of the equation of state further changes the location of the recurring region in radius, with softer EoSs reproducing smaller radii (and tidal deformability).

Once our neutron star observations, both electromagnetic and gravitational, become more accurate, our method could be used, for example, to produce different equations of state that reproduce measured neutron stars with a given mass and radii or neutron star mergers with a given mass and tidal deformability. Furthermore, in a neutron-star merger simulation, using different EoSs with similar macroscopic properties could allow us to make comparisons only based on the EoS structure. This would be of interest in studying the post-merger gravitational wave signal and inspiral signal from mergers, which could lead to a significant improvement of our understanding of dense matter. This could then provide predictions for future gravitational wave detectors in their search for evidence of stable quark matter in neutron stars. Work along those lines is in progress and will be reported soon.

Finally, note that this is an exploratory study. In the future, one could explore in a more consistent manner the size of the recurring region by using many more microscopic EoSs. This would require a more robust TOV solver (e.g., the one made available by the MUSES collaboration [Reinke Pelicer et al. \(2025\)](#)), as the interpolation error in the mass-radius curves can propagate into both the numerator and denominator of the speed of sound average, and a statistical approach such as Bayesian analysis.

Our work accompanies an open source script, that allows users to 1) create EoSs with percolation using different tabulated hadronic and quark EoS or tabulated hybrid EoS (in CompOSE format), 2) determine a recurring region for a given chosen stellar mass for that EoS, and 3) test different hadronic EoSs in order to modify the recurring region radius and tidal deformability. CMF 1-7 EoSs [Clevinger et al. \(2022\)](#) available on the CompOSE repository [Oertel et al. \(2017\)](#); [Typel et al. \(2015\)](#); [Oertel et al. \(2017\)](#); [Typel et al. \(2022, 2015\)](#), for example, provide small variations of the CMF model and could be used for such exploration. The link to the Python scripts will be added upon publication.

5. ACKNOWLEDGMENTS

This work is partially supported by the NP3M Focused Research Hub supported by the National Science Foundation (NSF) under grant No. PHY-2116686. VD also acknowledges support from the Fulbright U.S.

Scholar Program and the Department of Energy under grant DE-SC0024700. ZL and AWS were supported by NSFPHY21-16686. AWS was also supported by the De-

partment of Energy Office of Nuclear Physics. MA expresses sincere gratitude to the FCT for their generous support through Ph.D. grant number 2022.11685.BD (DOI: <https://doi.org/10.54499/2022.11685.BD>).

REFERENCES

- Alford, M., & Sedrakian, A. 2017, *Physical Review Letters*, 119, doi: [10.1103/physrevlett.119.161104](https://doi.org/10.1103/physrevlett.119.161104)
- Aloy, M. A., Ibáñez, J. M., Sanchis-Gual, N., et al. 2019, *Mon. Not. Roy. Astron. Soc.*, 484, 4980, doi: [10.1093/mnras/stz293](https://doi.org/10.1093/mnras/stz293)
- Altiparmak, S., Ecker, C., & Rezzolla, L. 2022, *The Astrophysical Journal Letters*, 939, L34, doi: [10.3847/2041-8213/ac9b2a](https://doi.org/10.3847/2041-8213/ac9b2a)
- Alvarez-Castillo, D., Ayriyan, A., Benic, S., et al. 2016, *Eur. Phys. J. A*, 52, 69, doi: [10.1140/epja/i2016-16069-2](https://doi.org/10.1140/epja/i2016-16069-2)
- Alvarez-Castillo, D., Blaschke, D., Grunfeld, A., & Pagura, V. 2019, *Physical Review D*, 99, doi: [10.1103/physrevd.99.063010](https://doi.org/10.1103/physrevd.99.063010)
- Annala, E., Gorda, T., Kurkela, A., Nättilä, J., & Vuorinen, A. 2020, *Nature Physics*, 16, 907, doi: [10.1038/s41567-020-0914-9](https://doi.org/10.1038/s41567-020-0914-9)
- Bastian, N.-U. F. 2021, *Physical Review D*, 103, doi: [10.1103/physrevd.103.023001](https://doi.org/10.1103/physrevd.103.023001)
- Baym, G., Furusawa, S., Hatsuda, T., Kojo, T., & Togashi, H. 2019, *Astrophys. J.*, 885, 42, doi: [10.3847/1538-4357/ab441e](https://doi.org/10.3847/1538-4357/ab441e)
- Baym, G., Hatsuda, T., Kojo, T., et al. 2018, *Rept. Prog. Phys.*, 81, 056902, doi: [10.1088/1361-6633/aaae14](https://doi.org/10.1088/1361-6633/aaae14)
- Bedaque, P., & Steiner, A. W. 2015, *Phys. Rev. Lett.*, 114, 031103, doi: [10.1103/PhysRevLett.114.031103](https://doi.org/10.1103/PhysRevLett.114.031103)
- Blaschke, D., Grigorian, H., & Röpke, G. 2020, *Particles*, 3, 477–499, doi: [10.3390/particles3020033](https://doi.org/10.3390/particles3020033)
- Braun, J., & Schallmo, B. 2022, Zero-temperature thermodynamics of dense asymmetric strong-interaction matter. <https://arxiv.org/abs/2204.00358>
- Clevinger, A., Corkish, J., Aryal, K., & Dexheimer, V. 2022, *Eur. Phys. J. A*, 58, 96, doi: [10.1140/epja/s10050-022-00745-3](https://doi.org/10.1140/epja/s10050-022-00745-3)
- Cuceu, I., & Robles, S. 2025, *Physical Review D*, 111, doi: [10.1103/6d9c-c4kx](https://doi.org/10.1103/6d9c-c4kx)
- De, S., Finstad, D., Lattimer, J. M., et al. 2018, *Phys. Rev. Lett.*, 121, 091102, doi: [10.1103/PhysRevLett.121.091102](https://doi.org/10.1103/PhysRevLett.121.091102)
- de Paoli, M. G., & Menezes, D. P. 2013, in *AIP Conference Proceedings (AIP)*, 217–224, doi: [10.1063/1.4804121](https://doi.org/10.1063/1.4804121)
- Dexheimer, V., Gomes, R. O., Klähn, T., Han, S., & Salinas, M. 2021, *Phys. Rev. C*, 103, 025808, doi: [10.1103/PhysRevC.103.025808](https://doi.org/10.1103/PhysRevC.103.025808)
- Dexheimer, V., Negreiros, R., & Schramm, S. 2015, *Physical Review C*, 91, doi: [10.1103/physrevc.91.055808](https://doi.org/10.1103/physrevc.91.055808)
- Dexheimer, V., & Schramm, S. 2008, *Astrophys. J.*, 683, 943, doi: [10.1086/589735](https://doi.org/10.1086/589735)
- Dexheimer, V. A., & Schramm, S. 2010, *Phys. Rev. C*, 81, 045201, doi: [10.1103/PhysRevC.81.045201](https://doi.org/10.1103/PhysRevC.81.045201)
- Duarte, D. C., Hernandez-Ortiz, S., & Jeong, K. S. 2020, *Phys. Rev. C*, 102, 025203, doi: [10.1103/PhysRevC.102.025203](https://doi.org/10.1103/PhysRevC.102.025203)
- Dutra, M., Lourenço, O., & Menezes, D. P. 2016, *Physical Review C*, 93, doi: [10.1103/physrevc.93.025806](https://doi.org/10.1103/physrevc.93.025806)
- Dutra, M., Lourenço, O., Sá Martins, J. S., et al. 2012, *Physical Review C*, 85, doi: [10.1103/physrevc.85.035201](https://doi.org/10.1103/physrevc.85.035201)
- Fadafan, K. B., Rojas, J. C., & Evans, N. 2020, *Physical Review D*, 101, doi: [10.1103/physrevd.101.126005](https://doi.org/10.1103/physrevd.101.126005)
- Ferreira, M., Pereira, R. C., & Providência, C. 2020, *Physical Review D*, 102, doi: [10.1103/physrevd.102.083030](https://doi.org/10.1103/physrevd.102.083030)
- Fonseca, E., et al. 2021, *Astrophys. J. Lett.*, 915, L12, doi: [10.3847/2041-8213/ac03b8](https://doi.org/10.3847/2041-8213/ac03b8)
- Fraga, E. S., da Mata, R., Pitsinikos, S., & Schmitt, A. 2022, Strange quark matter from a baryonic approach. <https://arxiv.org/abs/2206.09219>
- Fujimoto, Y., Fukushima, K., McLerran, L. D., & Praszalowicz, M. 2022, *Phys. Rev. Lett.*, 129, 252702, doi: [10.1103/PhysRevLett.129.252702](https://doi.org/10.1103/PhysRevLett.129.252702)
- Gao, B., Yan, Y., & Harada, M. 2024, Reconciling the HESS J1731-347 constraints with Parity doublet model. <https://arxiv.org/abs/2404.04786>
- Guichon, P. A., Saito, K., Rodionov, E., & Thomas, A. W. 1996, *Nuclear Physics A*, 601, 349–379, doi: [10.1016/0375-9474\(96\)00033-4](https://doi.org/10.1016/0375-9474(96)00033-4)
- Gulminelli, F., & Raduta, A. R. 2015, *Phys. Rev. C*, 92, 055803, doi: [10.1103/PhysRevC.92.055803](https://doi.org/10.1103/PhysRevC.92.055803)
- Gusakov, M. E., Haensel, P., & Kantor, E. M. 2014, *Monthly Notices of the Royal Astronomical Society*, 439, 318–333, doi: [10.1093/mnras/stt2438](https://doi.org/10.1093/mnras/stt2438)
- Han, M.-Z., Huang, Y.-J., Tang, S.-P., & Fan, Y.-Z. 2023, *Science Bulletin*, 68, 913–919, doi: [10.1016/j.scib.2023.04.007](https://doi.org/10.1016/j.scib.2023.04.007)
- Hempel, M., & Schaffner-Bielich, J. 2010, *Nucl. Phys. A*, 837, 210, doi: [10.1016/j.nuclphysa.2010.02.010](https://doi.org/10.1016/j.nuclphysa.2010.02.010)

- Hinderer, T. 2008, *Astrophys. J.*, 677, 1216, doi: [10.1086/533487](https://doi.org/10.1086/533487)
- Hippert, M., Fraga, E. S., & Noronha, J. 2021, *Phys. Rev. D*, 104, 034011, doi: [10.1103/PhysRevD.104.034011](https://doi.org/10.1103/PhysRevD.104.034011)
- Huang, K., Hu, J., Zhang, Y., & Shen, H. 2022, *The Astrophysical Journal*, 935, 88, doi: [10.3847/1538-4357/ac7f3c](https://doi.org/10.3847/1538-4357/ac7f3c)
- Ivanytskyi, O., & Blaschke, D. 2022, *Physical Review D*, 105, doi: [10.1103/physrevd.105.114042](https://doi.org/10.1103/physrevd.105.114042)
- Jakobus, P., Motornenko, A., Gomes, R. O., Steinheimer, J., & Stoecker, H. 2021, *The European Physical Journal C*, 81, doi: [10.1140/epjc/s10052-020-08779-x](https://doi.org/10.1140/epjc/s10052-020-08779-x)
- Jeong, K. S., McLerran, L., & Sen, S. 2020, *Physical Review C*, 101, doi: [10.1103/physrevc.101.035201](https://doi.org/10.1103/physrevc.101.035201)
- Jin, H.-M., Xia, C.-J., Sun, T.-T., & Peng, G.-X. 2022, *Physics Letters B*, 829, 137121, doi: [10.1016/j.physletb.2022.137121](https://doi.org/10.1016/j.physletb.2022.137121)
- Jokela, N., Järvinen, M., Nijs, G., & Remes, J. 2021, *Physical Review D*, 103, doi: [10.1103/physrevd.103.086004](https://doi.org/10.1103/physrevd.103.086004)
- Kaltenborn, M. A. R., Bastian, N.-U. F., & Blaschke, D. B. 2017, *Phys. Rev. D*, 96, 056024, doi: [10.1103/PhysRevD.96.056024](https://doi.org/10.1103/PhysRevD.96.056024)
- Kapusta, J. I., & Welle, T. 2021, *Physical Review C*, 104, doi: [10.1103/physrevc.104.1012801](https://doi.org/10.1103/physrevc.104.1012801)
- Kawaguchi, M., & Suenaga, D. 2024, *Physical Review D*, 109, doi: [10.1103/physrevd.109.096034](https://doi.org/10.1103/physrevd.109.096034)
- Kojo, T. 2019, in *XIAMEN-CUSTIPEN WORKSHOP ON THE EQUATION OF STATE OF DENSE NEUTRON-RICH MATTER IN THE ERA OF GRAVITATIONAL WAVE ASTRONOMY*, Vol. 2127 (AIP Publishing), 020023, doi: [10.1063/1.5117813](https://doi.org/10.1063/1.5117813)
- Kojo, T. 2021, QCD equations of state and speed of sound in neutron stars. <https://arxiv.org/abs/2011.10940>
- Kojo, T., Powell, P. D., Song, Y., & Baym, G. 2015, *Phys. Rev. D*, 91, 045003, doi: [10.1103/PhysRevD.91.045003](https://doi.org/10.1103/PhysRevD.91.045003)
- Kouno, H., & Kashiwa, K. 2024, Hadron-quark transition and chiral symmetry restoration at high density. <https://arxiv.org/abs/2310.09738>
- Kovács, P., Takátsy, J., Schaffner-Bielich, J., & Wolf, G. 2022, *Physical Review D*, 105, doi: [10.1103/physrevd.105.103014](https://doi.org/10.1103/physrevd.105.103014)
- Kumar, A., Dey, D., Haque, S., Mallick, R., & Patra, S. K. 2023a, Quarkyonic Model for Neutron Star Matter: A Relativistic Mean-Field Approach. <https://arxiv.org/abs/2304.08223>
- Kumar, D., Mishra, H., & Malik, T. 2023b, Non-radial oscillation modes in hybrid stars: consequences of a mixed phase. <https://arxiv.org/abs/2110.00324>
- Kumar, R., et al. 2023c, Theoretical and Experimental Constraints for the Equation of State of Dense and Hot Matter. <https://arxiv.org/abs/2303.17021>
- Lee, H. K., Ma, Y.-L., Paeng, W.-G., & Rho, M. 2022, *Modern Physics Letters A*, 37, doi: [10.1142/s0217732322300038](https://doi.org/10.1142/s0217732322300038)
- Legred, I., Chatziioannou, K., Essick, R., & Landry, P. 2022, *Physical Review D*, 105, doi: [10.1103/physrevd.105.043016](https://doi.org/10.1103/physrevd.105.043016)
- Li, A., Zhu, Z.-Y., Zhou, E.-P., et al. 2020a, *Journal of High Energy Astrophysics*, 28, 19–46, doi: [10.1016/j.jheap.2020.07.001](https://doi.org/10.1016/j.jheap.2020.07.001)
- Li, C.-M., Zhang, J.-L., Yan, Y., Huang, Y.-F., & Zong, H.-S. 2018, *Physical Review D*, 97, doi: [10.1103/physrevd.97.103013](https://doi.org/10.1103/physrevd.97.103013)
- Li, J. J., Sedrakian, A., & Alford, M. 2020b, *Physical Review D*, 101, doi: [10.1103/physrevd.101.063022](https://doi.org/10.1103/physrevd.101.063022)
- Liu, H., Yang, Y.-H., Han, Y., & Chu, P.-C. 2023, *Physical Review D*, 108, doi: [10.1103/physrevd.108.034004](https://doi.org/10.1103/physrevd.108.034004)
- Lopes, L. L., & Menezes, D. P. 2021, *Nuclear Physics A*, 1009, 122171, doi: [10.1016/j.nuclphysa.2021.122171](https://doi.org/10.1016/j.nuclphysa.2021.122171)
- Malfatti, G., Orsaria, M. G., Contrera, G. A., Weber, F., & Ranea-Sandoval, I. F. 2019, *Physical Review C*, 100, doi: [10.1103/physrevc.100.015803](https://doi.org/10.1103/physrevc.100.015803)
- Malfatti, G., Orsaria, M. G., Ranea-Sandoval, I. F., Contrera, G. A., & Weber, F. 2020, *Physical Review D*, 102, doi: [10.1103/physrevd.102.063008](https://doi.org/10.1103/physrevd.102.063008)
- Marczenko, M. 2020, *The European Physical Journal Special Topics*, 229, 3651–3661, doi: [10.1140/epjst/e2020-000093-3](https://doi.org/10.1140/epjst/e2020-000093-3)
- Marczenko, M., Redlich, K., & Sasaki, C. 2022, *The Astrophysical Journal Letters*, 925, L23, doi: [10.3847/2041-8213/ac4b61](https://doi.org/10.3847/2041-8213/ac4b61)
- McLerran, L. 2020, *Acta Phys. Polon. B*, 51, 1067, doi: [10.5506/APhysPolB.51.1067](https://doi.org/10.5506/APhysPolB.51.1067)
- McLerran, L., & Pisarski, R. D. 2007, *Nucl. Phys. A*, 796, 83, doi: [10.1016/j.nuclphysa.2007.08.013](https://doi.org/10.1016/j.nuclphysa.2007.08.013)
- McLerran, L., & Reddy, S. 2019, *Physical Review Letters*, 122, doi: [10.1103/physrevlett.122.122701](https://doi.org/10.1103/physrevlett.122.122701)
- Miller, M. C., et al. 2019, *Astrophys. J. Lett.*, 887, L24, doi: [10.3847/2041-8213/ab50c5](https://doi.org/10.3847/2041-8213/ab50c5)
- . 2021, *Astrophys. J. Lett.*, 918, L28, doi: [10.3847/2041-8213/ac089b](https://doi.org/10.3847/2041-8213/ac089b)
- Minamikawa, T., Kojo, T., & Harada, M. 2021, *Physical Review C*, 103, doi: [10.1103/physrevc.103.045205](https://doi.org/10.1103/physrevc.103.045205)
- Montaña, G., Tolós, L., Hanauske, M., & Rezzolla, L. 2019, *Physical Review D*, 99, doi: [10.1103/physrevd.99.103009](https://doi.org/10.1103/physrevd.99.103009)
- Motornenko, A., Steinheimer, J., Vovchenko, V., Schramm, S., & Stoecker, H. 2020, *Phys. Rev. C*, 101, 034904, doi: [10.1103/PhysRevC.101.034904](https://doi.org/10.1103/PhysRevC.101.034904)

- Mroczek, D., Miller, M. C., Noronha-Hostler, J., & Yunes, N. 2023, Nontrivial features in the speed of sound inside neutron stars. <https://arxiv.org/abs/2309.02345>
- Mukherjee, A., Schramm, S., Steinheimer, J., & Dexheimer, V. 2017, *Astronomy & Astrophysics*, 608, A110, doi: [10.1051/0004-6361/201731505](https://doi.org/10.1051/0004-6361/201731505)
- Nambu, Y., & Jona-Lasinio, G. 1961, *Phys. Rev.*, 122, 345, doi: [10.1103/PhysRev.122.345](https://doi.org/10.1103/PhysRev.122.345)
- Navas, S., et al. 2024, *Phys. Rev. D*, 110, 030001, doi: [10.1103/PhysRevD.110.030001](https://doi.org/10.1103/PhysRevD.110.030001)
- Oertel, M., Hempel, M., Klähn, T., & Typel, S. 2017, *Rev. Mod. Phys.*, 89, 015007, doi: [10.1103/RevModPhys.89.015007](https://doi.org/10.1103/RevModPhys.89.015007)
- Oppenheimer, J. R., & Volkoff, G. M. 1939, *Phys. Rev.*, 55, 374, doi: [10.1103/PhysRev.55.374](https://doi.org/10.1103/PhysRev.55.374)
- Pinto, M. B. 2023, *Physical Review C*, 107, doi: [10.1103/physrevc.107.045807](https://doi.org/10.1103/physrevc.107.045807)
- Pisarski, R. D. 2021, *Phys. Rev. D*, 103, L071504, doi: [10.1103/PhysRevD.103.L071504](https://doi.org/10.1103/PhysRevD.103.L071504)
- Raduta, A. R., Nacu, F., & Oertel, M. 2021, *The European Physical Journal A*, 57, doi: [10.1140/epja/s10050-021-00628-z](https://doi.org/10.1140/epja/s10050-021-00628-z)
- Raithel, C., Özel, F., & Psaltis, D. 2018, *Astrophys. J. Lett.*, 857, L23, doi: [10.3847/2041-8213/aabcbf](https://doi.org/10.3847/2041-8213/aabcbf)
- Reinke Pelicer, M., et al. 2025, *Phys. Rev. D*, 111, 103037, doi: [10.1103/PhysRevD.111.103037](https://doi.org/10.1103/PhysRevD.111.103037)
- Rho, M. 2021, Fractionalized Quasiparticles in Dense Baryonic Matter. <https://arxiv.org/abs/2004.09082>
- Riley, T. E., et al. 2019, *Astrophys. J. Lett.*, 887, L21, doi: [10.3847/2041-8213/ab481c](https://doi.org/10.3847/2041-8213/ab481c)
- . 2021, *Astrophys. J. Lett.*, 918, L27, doi: [10.3847/2041-8213/ac0a81](https://doi.org/10.3847/2041-8213/ac0a81)
- Saes, J. A., Mendes, R. F. P., & Yunes, N. 2024, *Phys. Rev. D*, 110, 024011, doi: [10.1103/PhysRevD.110.024011](https://doi.org/10.1103/PhysRevD.110.024011)
- Sen, D. 2021, *Physical Review C*, 103, doi: [10.1103/physrevc.103.045804](https://doi.org/10.1103/physrevc.103.045804)
- Sen, S., & Sivertsen, L. 2021, *Astrophys. J.*, 915, 109, doi: [10.3847/1538-4357/abff4c](https://doi.org/10.3847/1538-4357/abff4c)
- Sen, S., & Warrington, N. C. 2021, *Nuclear Physics A*, 1006, 122059, doi: [10.1016/j.nuclphysa.2020.122059](https://doi.org/10.1016/j.nuclphysa.2020.122059)
- Shahrbaf, M., Blaschke, D., Grunfeld, A. G., & Moshfegh, H. R. 2020, *Physical Review C*, 101, doi: [10.1103/physrevc.101.025807](https://doi.org/10.1103/physrevc.101.025807)
- Somasundaram, R., & Margueron, J. 2022, *Europhysics Letters*, 138, 14002, doi: [10.1209/0295-5075/ac63de](https://doi.org/10.1209/0295-5075/ac63de)
- Stone, J. R., Dexheimer, V., Guichon, P. A. M., Thomas, A. W., & Typel, S. 2021a, *Mon. Not. Roy. Astron. Soc.*, 502, 3476, doi: [10.1093/mnras/staa4006](https://doi.org/10.1093/mnras/staa4006)
- . 2021b, *Monthly Notices of the Royal Astronomical Society*, 502, 3476–3490, doi: [10.1093/mnras/staa4006](https://doi.org/10.1093/mnras/staa4006)
- Tajima, H., Iida, K., Kojo, T., & Liang, H. 2024, Tripling Fluctuations and Peaked Sound Speed in Fermionic Matter. <https://arxiv.org/abs/2412.04971>
- Tan, H., Dexheimer, V., Noronha-Hostler, J., & Yunes, N. 2022a, *Phys. Rev. Lett.*, 128, 161101, doi: [10.1103/PhysRevLett.128.161101](https://doi.org/10.1103/PhysRevLett.128.161101)
- Tan, H., Dore, T., Dexheimer, V., Noronha-Hostler, J., & Yunes, N. 2022b, *Phys. Rev. D*, 105, 023018, doi: [10.1103/PhysRevD.105.023018](https://doi.org/10.1103/PhysRevD.105.023018)
- Tews, I., Carlson, J., Gandolfi, S., & Reddy, S. 2018, *Astrophys. J.*, 860, 149, doi: [10.3847/1538-4357/aac267](https://doi.org/10.3847/1538-4357/aac267)
- Tolman, R. C. 1939, *Phys. Rev.*, 55, 364, doi: [10.1103/PhysRev.55.364](https://doi.org/10.1103/PhysRev.55.364)
- Tu, Z.-H., & Zhou, S.-G. 2022, *The Astrophysical Journal*, 925, 16, doi: [10.3847/1538-4357/ac3996](https://doi.org/10.3847/1538-4357/ac3996)
- Typel, S., Oertel, M., & Klähn, T. 2015, *Phys. Part. Nucl.*, 46, 633, doi: [10.1134/S1063779615040061](https://doi.org/10.1134/S1063779615040061)
- Typel, S., et al. 2022, *Eur. Phys. J. A*, 58, 221, doi: [10.1140/epja/s10050-022-00847-y](https://doi.org/10.1140/epja/s10050-022-00847-y)
- wu Wang, Q., Shi, C., Yan, Y., & Zong, H.-S. 2020, Exploring hybrid equation of state with constraints from tidal deformability of GW170817. <https://arxiv.org/abs/1912.02312>
- Xia, C., Zhu, Z., Zhou, X., & Li, A. 2021, *Chinese Physics C*, 45, 055104, doi: [10.1088/1674-1137/abea0d](https://doi.org/10.1088/1674-1137/abea0d)
- Xia, C.-J., Xie, W.-J., & Bakhiet, M. 2024, Astrophysical constraints on nuclear EOSs and coupling constants in RMF models. <https://arxiv.org/abs/2411.07170>
- Yamamoto, Y., Yasutake, N., & Rijken, T. A. 2023, Quark phases in neutron stars consistent with implications of NICER. <https://arxiv.org/abs/2309.10233>
- Yazdizadeh, T., & Bordbar, G. H. 2019, *Iranian Journal of Science and Technology, Transactions A: Science*, 43, 2691–2698, doi: [10.1007/s40995-019-00731-3](https://doi.org/10.1007/s40995-019-00731-3)
- Ye, J.-T., Wang, R., Wang, S.-P., & Chen, L.-W. 2025, High density symmetry energy: A key to the solution of the hyperon puzzle. <https://arxiv.org/abs/2411.18349>
- Zacchi, A., Hanauske, M., & Schaffner-Bielich, J. 2016, *Physical Review D*, 93, doi: [10.1103/physrevd.93.065011](https://doi.org/10.1103/physrevd.93.065011)
- Zhao, T., & Lattimer, J. M. 2020, *Physical Review D*, 102, doi: [10.1103/physrevd.102.023021](https://doi.org/10.1103/physrevd.102.023021)
- Zuo, B.-J., Huang, Y.-F., & Feng, H.-T. 2022, *Physical Review D*, 105, doi: [10.1103/physrevd.105.074011](https://doi.org/10.1103/physrevd.105.074011)

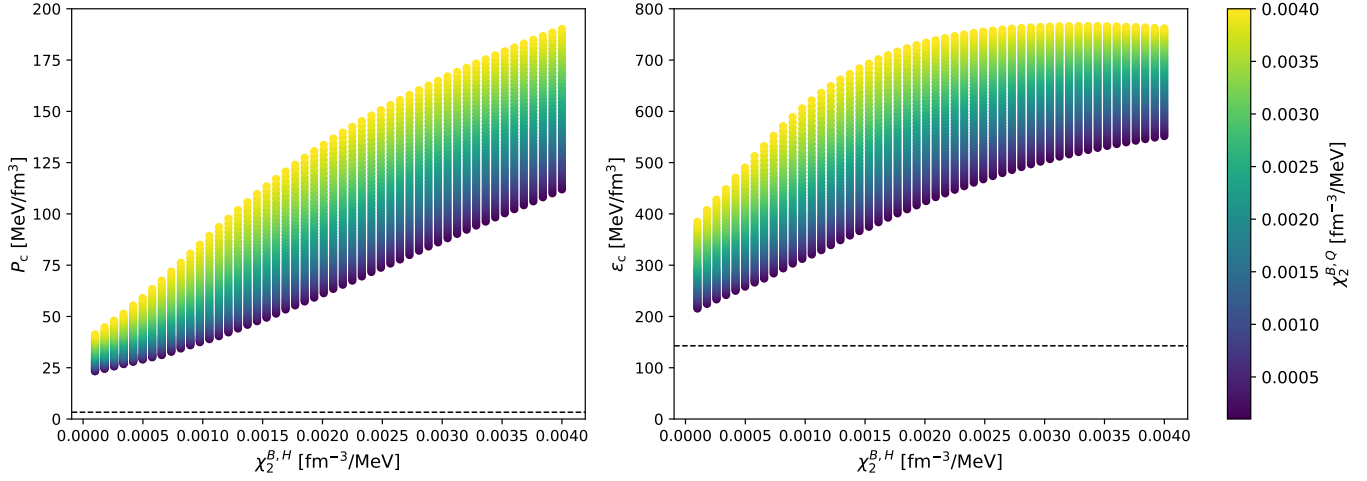


Figure B.1. Central stellar pressure (left) and central stellar energy density (right) as functions of the second-order susceptibility at the hadronic boundary of the percolation region. The colored scattering points show the second-order susceptibility at the quark boundary of the percolation region and the black dotted lines show the pressure (left) and energy density (right) at the hadronic boundary. Same percolation parameters and chosen stellar mass used in Fig. 2.

APPENDIX

A. MOTIVATION FOR PERCOLATION

In the Introduction, we suggested that we expect exotic matter to appear in the cores of neutron stars. To get a general idea about deconfinement, in particular, we can do a simple estimation to see why this is important. We assume that we only have nucleons (protons and neutrons) in a given hard volume, V . We estimate the size of nucleons to have a radius of $0.84 - 0.86$ fm based on the measured proton charge radius, proton magnetic radius and neutron magnetic radius from PDG 2024 [Navas et al. \(2024\)](#), so we can compare the estimated number density of one nucleon to the baryon (number) densities probed in the interior of a neutron star. Expressing this as an inequality, we have $n_B < 1/V$. Using our estimate for the radius of a nucleon and roughly approximating a nucleon as a sphere, the density at which the neutron star is the same density as a nucleon is $0.38\text{--}0.40$ fm $^{-3}$. Beyond these densities, the nucleons would have to overlap and the description of degrees of freedom as simple baryons would not make sense anymore. Specifically, within high-mass neutron star cores, depending on model assumptions, one could reproduce densities two or three times this value (see Fig. 4 of [Tan et al. \(2022b\)](#) for the case of a first-order phase transition). In reality, even before the nucleons overlap, a more complex description of quark deconfinement is needed, which is exactly what the percolation description we apply in this work is meant to reproduce.

B. ADDITIONAL CASES AND DETAILS

B.1. Percolation parameters and neutron star properties

In this subsection, we illustrate the relationship between the key percolation parameters $\chi_2^{B,H}$ and $\chi_2^{B,Q}$ and neutron star properties (for a given mass). Fig. B.1 shows how both the central stellar pressure (left panel) and central stellar energy density (right panel) increase with increasing susceptibilities at the boundaries of the percolation region. We observe that P_c increases with both susceptibilities faster than ϵ_c . This characteristic is what qualitatively explains the appearance of the minimum point of c_{avg}^2 we discuss in the text. Quantitatively, the value of χ_2^B (on either side of the percolation region) corresponding to the minimum of c_{avg}^2 (Eq. 3) is determined by

$$\frac{\partial c_{avg}^2}{\partial \chi_2^B} = 0, \quad (B1)$$

$$(\epsilon_c - \epsilon_H) \frac{\partial P_c}{\partial \chi_2^B} = (P_c - P_H) \frac{\partial \epsilon_c}{\partial \chi_2^B}, \quad (B2)$$

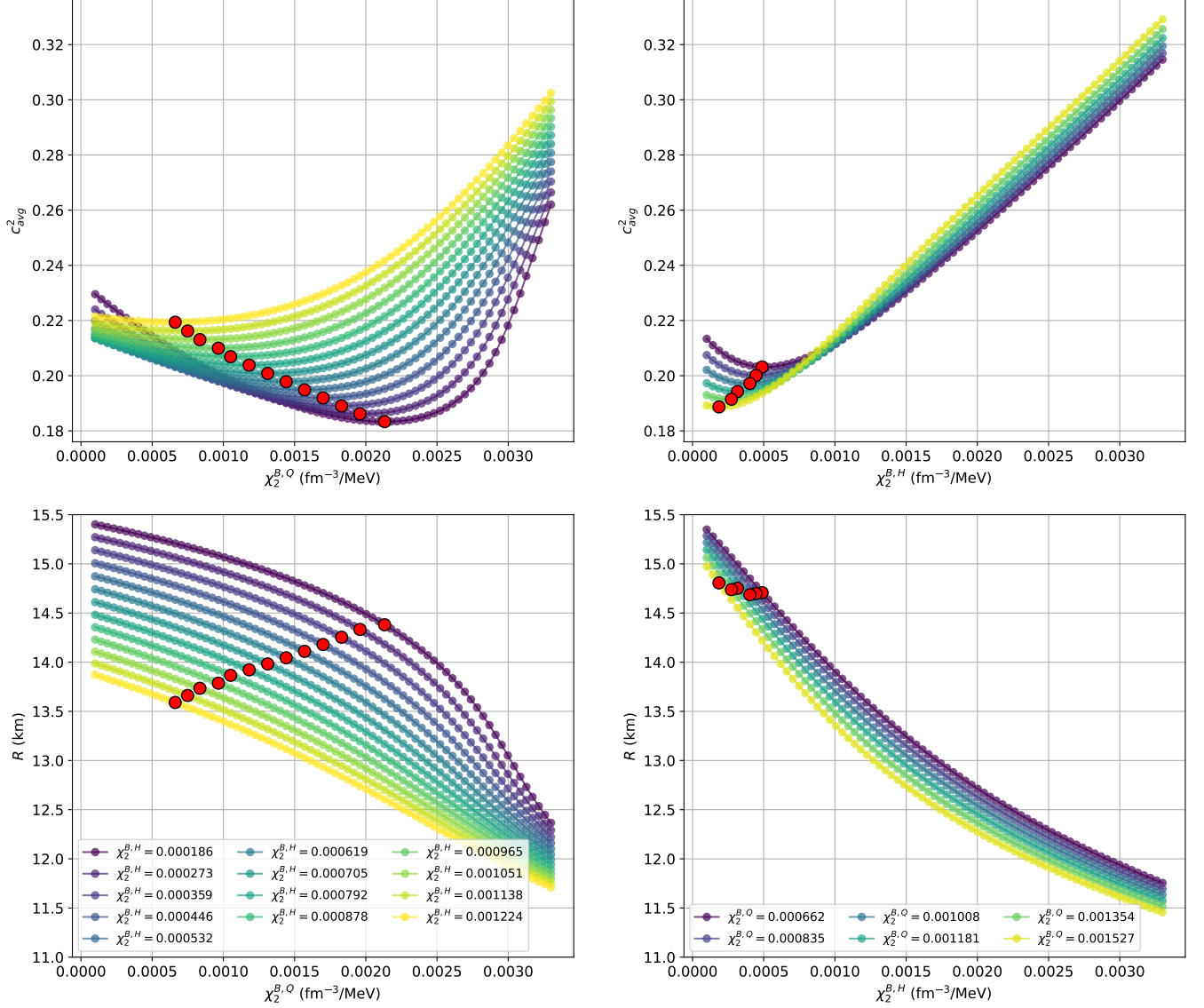


Figure B.2. Same percolation region parameters as Fig. 2 for CMF-7, except using a chosen stellar mass of $1.8 M_{\odot}$.

$$c_{\text{avg}}^2 = \frac{\partial P_c / \partial \chi_2^B}{\partial \varepsilon_c / \partial \chi_2^B}, \quad (\text{B3})$$

where the right side of Eq. B3 is given by the ratio of the slopes of both panels in Fig. B.1.

B.2. Higher mass stars

To further explore the flexibility of our approach, we apply the same prescription described in the text to find a recurring region for a higher chosen stellar mass of $1.8 M_{\odot}$. We show in Fig. B.2 recurring regions that appear at different radii in both cases, on the left panels showing the susceptibility at the quark boundary for the percolation in the x-axis and the different susceptibilities at the hadronic boundary using different line colors and on the right panels showing the susceptibilities exchanged. Looking at the red dots (that mark minima in the speed of sound squared in the top panels), the lower panels show that the radii are now larger (than for the smaller star mass already discussed) in both panels. The radii in the right panel are too large in comparison with astrophysical data, but the radii in the left bottom panel for such a high mass are still reasonable [Riley et al. \(2021\)](#); [Miller et al. \(2021\)](#).

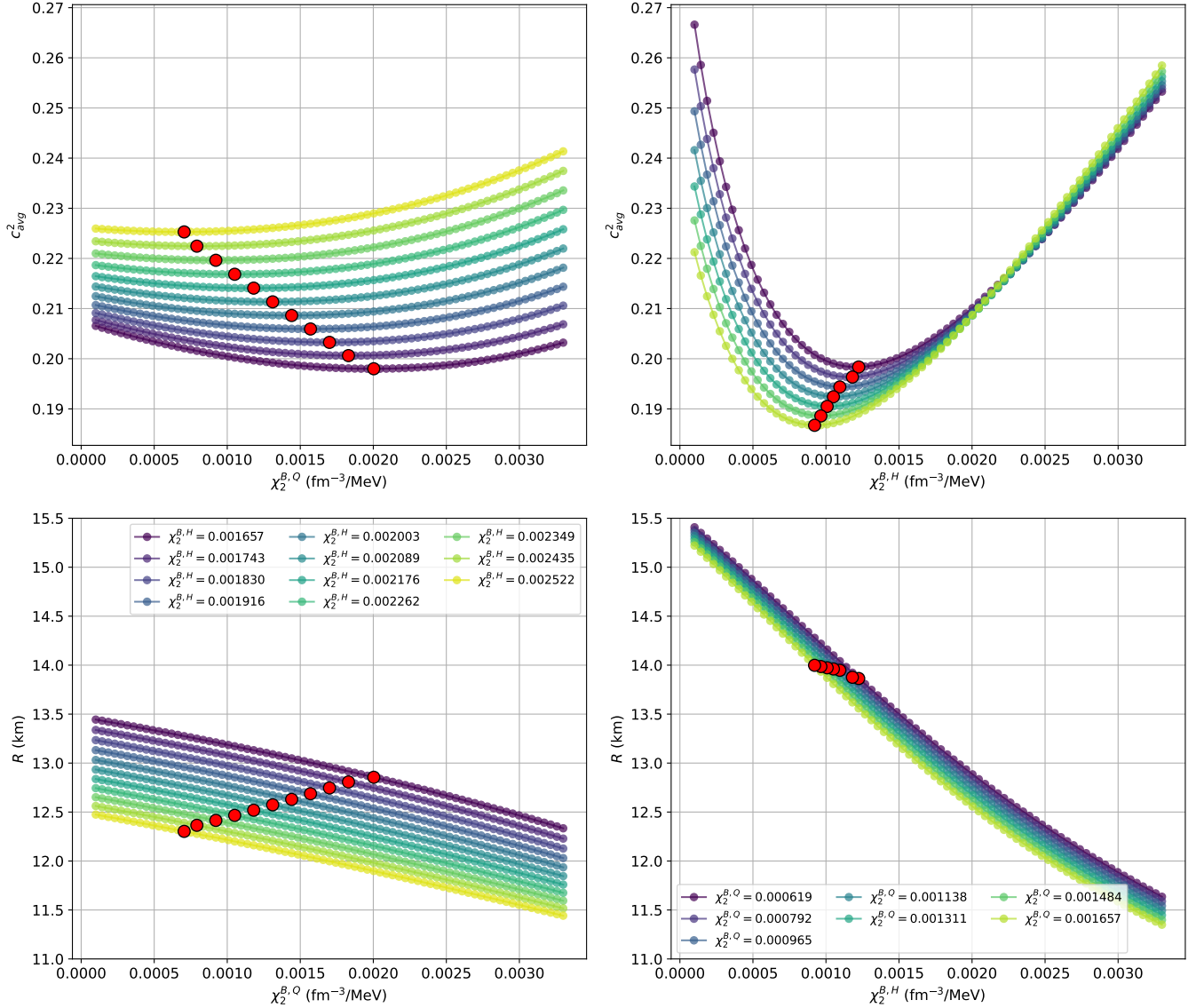


Figure B.3. Same percolation parameters and chosen stellar mass used in Fig. 2 but using the DD2F-NJL microscopic model rather than CMF-7.

B.3. Different microscopic model

The phenomenon of recurring regions we discuss in this work is not unique to the CMF model. We show in Fig. B.3 that we can also obtain recurring regions using the DD2F-NJL model, again for an example mass of $1.554 M_\odot$. The percolation densities are the same as in Fig. 2 ($n_{B,H} = 0.15$ and $n_{B,Q} = 1.2$ fm⁻³). The radius for the recurring region occurs at different values, but still not too different from the ones in CMF-7. Furthermore, all the curves in Fig. 2 and Fig. B.3 have the same qualitative shape. We note however that these EoSs present a softer hadronic component, which has the effect of lowering the radius of the recurring region in the left panels but having little effect on the right panels. These results show that using different microscopic models provide a way to tune the location of recurring regions, not only in mass, but also in radii and tidal deformability (related to radius De et al. (2018); Raithel et al. (2018)).